The Silicides YT_2Si_2 (T = Co, Ni, Cu, Ru, Rh, Pd): A Systematic Study by ^{89}Y Solid-state NMR Spectroscopy

Christoph Höting[a], Hellmut Eckert[b], Samir F. Matar[c], Ute Ch. Rodewald[a], and Rainer Pöttgen[a]

[a] Institut für Anorganische und Analytische Chemie, Universität Münster, Corrensstraße 30, D-48149 Münster, Germany

[b] Institut für Physikalische Chemie, Universität Münster, Corrensstraße 30, D-48149 Münster, Germany

[c] CNRS, Université de Bordeaux, ICMCB, 87 Avenue Dr. A. Schweitzer, F-33608 Pessac-Cedex, France

Reprint requests to R. Pöttgen. E-mail: pottgen@uni-muenster.de

Z. Naturforsch. **2014**, *69b*, 305 – 312 / DOI: 10.5560/ZNB.2014-3319
Received December 9, 2013

The $ThCr_2Si_2$-type silicides YT_2Si_2 (T = Co, Ni, Cu, Ru, Rh, Pd) were synthesized from the elements by arc-melting. They were characterized by powder X-ray diffraction, and the structures were refined on the basis of single-crystal X-ray diffractometer data. The course of the lattice parameters shows a distinct anomaly for YRu_2Si_2 which has by far the smallest c/a ratio along with elongated Y–Si distances. Systematic ^{89}Y solid-state NMR spectra show large Knight shifts arising from unpaired conduction electron spin density near the Fermi edge. The Knight shift decreases with increasing valence electron count (VEC), reflecting the sensitivity of this parameter to electronic properties. The particularly strong structural distortion observed in YRu_2Si_2 manifests itself in a sizeable magnetic shielding anisotropy. Electronic structure calculations for YRu_2Si_2 and YRh_2Si_2 reveal similar projected density of states (PDOS) shapes with an energy upshift of the Fermi level in YRh_2Si_2 due to the extra electron brought in by Rh. As a consequence, the PDOS at the Fermi energy is twice as large in the Ru compound as in the Rh compound. While both compounds show the major bonding interaction within the T_2Si_2 layers, YRh_2Si_2 exhibits significantly stronger Y–Si bonding.

Key words: Yttrium, Silicides, Crystal Structure, Solid-state NMR Spectroscopy

Introduction

The tetragonal $BaAl_4$ type [1], space group $I4/mmm$, and its ternary derivative $ThCr_2Si_2$ [2] are two of the most frequent structure types that occur for intermetallic compounds. The Pearson data base [3] lists several hundred representatives. The crystallographic details and the widely varying physical properties have been reviewed [4, 5]. The $ThCr_2Si_2$ derivatives of the general formula AT_2X_2 exist for many different element combinations. The A cation can be an alkali, alkaline earth, rare earth, or actinoid metal, and the whole series of transition metals has been observed on the T sites. The X sites can be occupied by elements of the 3rd, 4th and 5th main group. This flexibility in the site occupancies allows for variations of the valence electron count (VEC) and thus of the magnetic ground states. Especially the cerium- and uranium-containing phases have been studied extensively during the past thirty years in the context of heavy fermion systems [6, 7]. The same holds true for the europium and ytterbium compounds, whose electronic properties are characterized by valence fluctuations.

The AT_2X_2 phases show a wide range of c/a ratios [5], resulting from variations in the A, T, and X atomic size ratios. In addition, the lattice parameters also reflect variations in X–X bonding, depending on whether the X atoms are isolated or form covalently bonded X_2 dumb-bells. The simple formula $d_{X-X} = (0.16 + 0.04(c/a))c$ [8] allows an estimation of the X–X distance. These bonding peculiarities have been intensively studied by electronic structure calcu-

lations [9 – 11] with pioneering work done by the Hoffmann group.

Several of the AT_2X_2 phases show superconductivity at very low temperatures. Early work on YPt_2Si_2 [12], YIr_2Si_2 [13], YPd_2Si_2, and YRh_2Si_2 [14] revealed transition temperatures below 3 K. This field of research gained a true renaissance shortly after the discovery of superconductivity in the solid solution $Ba_{1-x}K_xFe_2As_2$ [15, 16] with $T_{max} = 38$ K. The extensive work on the superconductivity and charge density of AT_2X_2 phases has been reviewed by Johnston [17].

For developing an understanding of the electronic properties in terms of atomic composition and structure in intermetallic compounds, solid-state NMR spectroscopy is a useful tool, as the Knight shifts available from such measurements reflect unpaired conduction electron spin densities near the Fermi edge. Recently, we explored the potential of the ^{89}Y nucleus to gain such information for intermetallic compounds [18]. The isotypical series YT_2X_2 with its wide range of lattice parameters and electronic properties is an attractive candidate in this context. Herein we report on detailed crystallographic and ^{89}Y NMR spectroscopic trends observed for the silicides YT_2Si_2 with T = Co, Ni, Cu, Ru, Rh, Pd. These yttrium silicides were studied previously during investigations of the complete RET_2Si_2 series in order to manifest the nonmagnetic ground states of the $[T_2Si_2]$ networks (Table 1 [12 – 14, 19 – 31]).

Experimental

Synthesis

The starting materials for the preparation of the series of YT_2Si_2 (T = Co, Ni, Cu, Ru, Rh, Pd) samples were yttrium ingots (smart elements), lumps of cobalt (Alfa Aesar), nickel wire (Alfa Aesar), copper shots (Alfa Aesar), ruthenium, rhodium and palladium powder (Allgussa AG), and lumps of silicon (Strem Chemicals), all with a stated purity better than 99.9 %. Powdered elements were cold-pressed to pellets (⌀ 6 mm).

The elements were weighed in the stoichiometric ratio and arc-melted [32] in a dried argon atmosphere of about 700 mbar. The argon was purified over titanium sponge (900 K), silica gel, and molecular sieves. All buttons were turned over and remelted several times to ensure good homogeneity. The weight losses after several meltings were in all cases smaller than 0.5 %. The crushed buttons had a light-grey color with metallic luster. They are stable in air, and no decomposition was visible after several months.

X-Ray diffraction

The polycrystalline YT_2Si_2 samples were analyzed by powder X-ray diffraction using the Guinier technique (imaging plate detector, Fujifilm BAS-1800) with Cu$K_{\alpha1}$ radiation and α-quartz (a = 491.30 and c = 540.46 pm) as an internal standard. The tetragonal lattice parameters (Table 1) were deduced from least-squares fits. Our data are in agreement with literature values. Correct indexing was ensured through intensity calculations [33].

YT_2Si_2 single crystals were selected from the crushed samples. The crystals were fixed at thin quartz fibers using beeswax and investigated by Laue photographs in a Buerger camera (white molybdenum radiation; imaging plate technique, Fujifilm, BAS-1800). Intensity data of an YNi_2Si_2 crystal were collected at room temperature using a four-circle diffractometer (CAD4) with graphite-monochromatized MoK_α radiation and a scintillation counter with pulse height discrimination. Scans were taken in the $\omega/2\theta$ mode. The YCo_2Si_2, YRu_2Si_2 and YRh_2Si_2 crystals were measured on a Stoe IPDS-II imaging plate diffractometer in oscillation mode (graphite-monochromatized Mo radiation). Numerical absorption corrections were applied to

Table 1. Refined lattice parameters (Guinier powder data) of the silicides YT_2Si_2 (T = Co, Ni, Cu, Ru, Rh, Pd) with $ThCr_2Si_2$-type structure.

Compound	a (pm)	c (pm)	V (nm^3)	Reference
YCo_2Si_2	388.75(7)	973.4(3)	0.1471	this work
	396	978	0.1534	[27]
	389.2	975.9	0.1478	[23]
	389.04(6)	975.1(2)	0.1476	[26]
YNi_2Si_2	395.51(7)	956.8(2)	0.1497	this work
	395	953	0.1487	[30]
	395.6	953.5	0.1492	[24]
	396.4	959.9	0.1508	[25]
YCu_2Si_2	396.15(7)	995.9(2)	0.1563	this work
	396.7	995.9	0.1567	[24]
	396.75(7)	997.6(3)	0.1570	[20]
	396.7	995.9	0.1567	[21]
	397.06(2)	998.07(7)	0.1574	[27, 28]
YRu_2Si_2	415.80(6)	954.6(2)	0.1650	this work
	415.57(6)	953.7(3)	0.1647	[22]
	415.7(1)	952.2(3)	0.1645	[12]
YRh_2Si_2	401.81(9)	989.7(3)	0.1598	this work
	403.1	992	0.1612	[31]
	403.1(2)	992(1)	0.1612	[19]
	402.3(1)	990.0(6)	0.1602	[12]
	403.1	992.0	0.1612	[14]
YPd_2Si_2	412.77(3)	985.74(9)	0.1679	this work
	412.2	992	0.1685	[31]
	412.5(1)	984.2(4)	0.1675	[12]
	412.9	984	0.1678	[14]

Table 2. Crystal data and structure refinement for YT_2Si_2 (T = Co, Ni, Ru, Rh, Pd) with $ThCr_2Si_2$ structure type, space group $I4/mmm$, $Z = 2$.

Empirical formula	YCo_2Si_2	YNi_2Si_2	YRu_2Si_2	YRh_2Si_2	YPd_2Si_2
Molar mass, g mol^{-1}	262.9	262.5	347.2	350.9	357.9
Unit cell dimensions (Guinier powder data)					
a, pm	388.75(7)	395.51(7)	415.80(6)	401.81(9)	412.77(3)
c, pm	973.4(3)	956.8(2)	954.6(2)	989.7(3)	985.74(9)
Cell volume, nm^3	0.1471	0.1497	0.1650	0.1598	0.1679
Calculated density, g cm^{-3}	5.93	5.82	6.99	7.29	7.07
Crystal size, μm^3	$10 \times 15 \times 20$	$20 \times 20 \times 100$	$15 \times 20 \times 40$	$10 \times 15 \times 30$	$10 \times 10 \times 20$
Transm. ratio (max/min)	0.67/0.30	0.49/0.26	0.41/0.25	0.18/0.12	0.22/0.13
Diffractometer	IPDS II	CAD4	IPDS II	IPDS II	StadiVari
Detector distance, mm	60	–	60	60	60
Exposure time, sec	600	–	360	600	50
ω range/increment, deg	0 – 180/1.0	–	0 – 180/1.0	0 – 180/1.0	–
Integr. parameters A/B/EMS	13.2/2.9/0.012	–	12.7/2.8/0.011	12.9/2.9/0.013	8.6/8.0/0.03
Absorption coefficient, mm^{-1}	31.2	32.2	26.9	28.7	28.2
F(000), e	242	246	310	314	318
θ range, deg	4.2 – 34.8	4.3 – 49.8	4.3 – 34.7	4.1 – 34.9	5.4 – 40.0
Range in hkl	±6, ±6, +15	±8, ±8, +20	±6, ±6, +15	±6, ±6, +15	±7, ±7, ±17
Total no. reflections	633	1538	691	685	3046
Independent reflections/R_{int}	122/0.0467	264/0.0253	131/0.0208	131/0.0164	186/0.0451
Reflections with $I > 3\sigma(I)$	101/0.0250	247/0.0128	128/0.0101	128/0.0140	157/0.0257
Data/parameters	122/9	264/9	131/9	131/9	186/9
Goodness-of-fit on F^2	1.57	1.68	0.73	1.26	1.55
$R1/wR2$ for $I > 3\sigma(I)$	0.0274/0.0556	0.0176/0.0562	0.0088/0.0197	0.0138/0.0374	0.0281/0.0639
$R1/wR2$ for all data	0.0356/0.0569	0.0194/0.0565	0.0093/0.0198	0.0146/0.0375	0.0337/0.0654
Extinction coefficient	160(30)	100(20)	119(7)	128(12)	83(18)
Largest diff. peak/hole, e A^{-3}	2.44/ – 1.21	1.92/ – 1.09	0.32/ – 0.26	0.81/ – 0.66	1.64/ – 1.78

these four data sets. Data of the YPd_2Si_2 crystal were measured on a Stoe StadiVari system equipped with a Mo microfocus source and a Pilatus 100 K detector with a hybrid-pixel sensor. An empirical absorption correction was applied to this data set. Details about the data collections and the crystallographic parameters are summarized in Table 2.

Structure refinements

The systematic extinctions of the five data sets were in agreement with the centrosymmetric space group $I4/mmm$. The atomic positions of the aristotype $ThCr_2Si_2$ [2] were taken as starting values, and the structures were refined using the JANA2006 package [34, 35] with anisotropic atomic displacement parameters (ADPs) for all atoms. The occupancy parameters of all sites were refined in separate series of least-squares cycles. All sites were fully occupied within two standard deviations. The final difference Fourier synthesis showed no significant residual peaks. The refined atomic positions, the ADPs, and the interatomic distances are given in Tables 3 and 4.

Further details of the crystal structure investigation may be obtained from Fachinformationszentrum Karlsruhe, 76344 Eggenstein-Leopoldshafen, Germany (fax: +49-7247-808-666; e-mail: crysdata@fiz-karlsruhe.de, http://www.fiz-karlsruhe.de/request_for_deposited_data.html) on quoting the deposition number CSD-427109 (YCo_2Si_2), CSD-427110 (YNi_2Si_2), CSD-427111 (YRu_2Si_2), CSD-427112 (YRh_2Si_2), and CSD-427113 (YPd_2Si_2).

^{89}Y solid-state NMR spectroscopy

^{89}Y solid-state NMR spectra were measured on a Bruker DSX-500 spectrometer equipped with a 7 mm low-gamma magic-angle spinning (MAS) NMR probe (^{89}Y resonance frequency 24.5 MHz). To minimize probe detuning and rf sample heating effects of these metallic samples, intimate mixtures of the powdered material and α-quartz in a 1 : 1 mass ratio were investigated. Samples were rotated at the magic angle with rotation speeds of 5 – 7 kHz, and spectra were obtained in the form of Bloch decay signals, using 90° pulses of 9.5 μs length, and relaxation delays of 2 – 5 seconds. To suppress probe ringing effects, all the spectra were obtained following a pre-acquisition delay of one rotor period. Resonance shifts are reported relative to an external 1 M aqueous YCl_3 solution.

Computational details

Within the well-established quantum theoretical density functional theory (DFT) framework [36, 37] we used the

generalized gradient approximation GGA [38] for an account of the effects of exchange correlation. Based on DFT-GGA, calculations were carried out within the all electron scalar-relativistic augmented spherical wave (ASW) method [39, 40]. The method allows for a full description of the electronic structure and the properties of chemical bonding based on the analysis of the overlap integrals S_{ij} with the crystal orbital overlap populations COOP following Hoffmann [41]. In the plots, positive, negative, and zero COOP indicate bonding, anti-bonding and non-bonding interactions, respectively. Due to the limited basis set used in the ASW method, we chose the outermost shells to represent the valence states, and the matrix elements were constructed using partial waves up to $l_{max}+1=4$ for Y, $l_{max}+1=3$ for T and $l_{max}+1=2$ for Si. Self-consistency was achieved when charge transfers and energy changes between two successive cycles were below 10^{-8} and 10^{-6} eV, respectively. Brillouin zone integrations were performed using the linear tetrahedron method within the irreducible wedge.

Table 3. Atomic positions and anisotropic displacement parameters (pm^2) of YT_2Si_2 (T = Co, Ni, Cu, Ru, Rh, Pd), space group $I4/mmm$. The anisotropic displacement factor exponent takes the form: $-2\pi^2[(ha^*)^2U_{11}+\ldots+2hka^*b^*U_{12}]$; $U_{11}=U_{22}$; $U_{12}=U_{13}=U_{13}=0$; U_{eq} is defined as one third of the trace of the orthogonalized U_{ij} tensor.

Atom	Site	x	y	z	U_{11}	U_{33}	U_{eq}
YCo_2Si_2							
Y	2*a*	0	0	0	49(4)	61(5)	53(3)
Co	4*d*	0	1/2	1/4	47(4)	53(5)	49(2)
Si	4*e*	0	0	0.3731(3)	45(6)	55(9)	48(4)
YNi_2Si_2							
Y	2*a*	0	0	0	41(1)	60(2)	47(1)
Ni	4*d*	0	1/2	1/4	76(1)	65(2)	72(1)
Si	4*e*	0	0	0.3742(1)	59(2)	74(4)	64(2)
YCu_2Si_2 [27]							
Y	2*a*	0	0	0	–	–	–
Cu	4*d*	0	1/2	1/4	–	–	–
Si	4*e*	0	0	0.38314(18)	–	–	–
YRu_2Si_2							
Y	2*a*	0	0	0	58(1)	59(2)	58(1)
Ru	4*d*	0	1/2	1/4	28(1)	47(1)	34(1)
Si	4*e*	0	0	0.36837(9)	43(2)	52(3)	46(2)
YRh_2Si_2							
Y	2*a*	0	0	0	71(3)	76(3)	73(2)
Rh	4*d*	0	1/2	1/4	51(2)	72(2)	58(1)
Si	4*e*	0	0	0.3777(2)	67(5)	78(7)	71(3)
YPd_2Si_2							
Y	2*a*	0	0	0 149(4)	145(6)	148(3)	
Pd	4*d*	0	1/2	1/4	154(2)	157(3)	155(1)
Si	4*e*	0	0	0.3827(3)	157(8)	167(13)	160(6)

Table 4. Interatomic distances (pm) in the structures of YT_2Si_2 (T = Co, Ni, Cu, Ru, Rh, Pd). Standard deviations are all equal or less than 0.3 pm. All distances within the first coordination spheres are listed. The data of the copper compound were taken from ref. [27].

			YCo_2Si_2	YNi_2Si_2	YCu_2Si_2	YRu_2Si_2	YRh_2Si_2	YPd_2Si_2
Y	8	Si	301.4	304.5	304.0	319.7	308.8	313.9
	8	*T*	311.4	310.4	318.9	316.5	318.7	321.4
T	4	Si	228.3	230.7	238.9	236.6	237.4	244.3
	4	*T*	274.9	279.7	280.8	294.0	284.1	291.9
	4	Y	311.4	310.4	318.9	316.5	318.7	321.4
Si	4	*T*	228.3	230.7	238.9	236.6	237.4	231.3
	1	Si	247.1	240.8	233.3	251.3	242.0	244.3
	4	Y	301.4	304.5	304.0	319.7	308.8	313.9

Results and Discussion

Crystal chemistry

The crystal chemistry and chemical bonding of the various phases derived from the $ThCr_2Si_2$ structure has been summarized repeatedly [4, 5, 9–11, 42]. Herein we only focus on the details that are relevant for the yttrium-based silicides. The transition metal atoms have tetrahedral silicon coordination with T–Si distances close to the sums of the covalent radii [43]. Layers of edge-sharing $TSi_{4/4}$ tetrahedra (Fig. 1) are connected *via* Si–Si bonding. The Si–Si distances range from 233 pm in YCu_2Si_2 to 251 pm in YRu_2Si_2, typical for single bonds. The three-dimensional $[T_2Si_2]$ polyanionic networks leave larger cages which are filled by the yttrium atoms. Besides strong covalent T–Si and Si–Si bonding, there is evidence for weak T–T bonding [11]. The local environment of the yttrium atoms is characterized by two interpenetrating polygons with eight identical Y–Si and eight identical Y–T distances, where the ratio of these distances is reflected by the c/a lattice parameter ratio. Figure 2 shows the dependence of the cell volume on the nature of the transition metal, including all YT_2Si_2 compounds listed in the Pearson data base [3]. Similar to the family of ThT_2Si_2 silicides already reported in 1965 [3], the YT_2Si_2 series shows distinct minima in the cell volumina for the Co, Rh and Ir compounds, suggesting maximum bond strength in the compounds formed by T atoms of group IX. The c/a ratios (YCo_2Si_2: 2.504; YNi_2Si_2: 2.419; YCu_2Si_2: 2.514; YRu_2Si_2: 2.296; YRh_2Si_2: 2.463; YPd_2Si_2: 2.388) show by far the smallest value for YRu_2Si_2. This results in anomalously long Y–Si distances (320 pm), which are in this case even longer than the Y–Ru distances (317 pm). This reversal in the order of the closest nearest neighbors in YRu_2Si_2 as compared to all the other members in this series influences the bonding situation of the yttrium atoms, as discussed below on the basis of ^{89}Y solid-state NMR spectra and overlap populations.

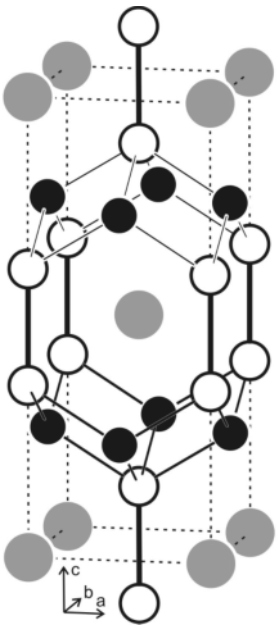

Fig. 1. The crystal structure of the silicides YT_2Si_2. Yttrium, transition metal and silicon atoms are drawn as medium grey, black filled and open circles, respectively. The three-dimensional $[T_2Si_2]$ network is emphasized.

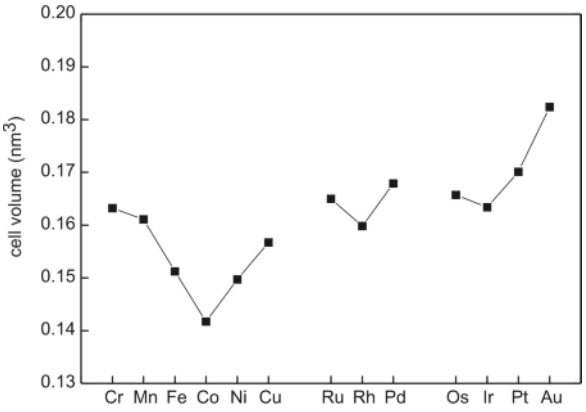

Fig. 2. Course of the cell volumes of the silicides YT_2Si_2 as a function of the atomic number of the transition metal. Data that are not listed in Table 1 were taken from the Pearson data base [3].

Electronic structure calculations for YRu_2Si_2 and YRh_2Si_2

Calculations assume spin degenerate (total spins) configuration, *i. e.* no spin polarization (NSP). At self-consistent convergence little charge transfer could be observed between the atomic species as it is the case for an intermetallic compound, the major effect being the quantum mixing between the valence states of the constituents within the valence band (VB). This is illustrated by the site projected density of states (PDOS) given in Fig. 3 for the two compounds as a function of the energy difference E–E_F, where E_F is the Fermi energy. The two panels show similar features pertain-

ing to Si (s, p) states low in energy, $-12 \leq (E–E_F) \leq -8$ eV, as well as for the low-energy part of the T (d) states. These features indicate the expected strong T–Si bonding interactions within the T_2Si_2 layers characterizing the structure. A major feature differentiating the two compounds which exhibit nearly similar DOS is the Fermi level upshift in YRh_2Si_2 due to the extra electron brought in by Rh. This leads to a doubling for Ru(PDOS) *vs*. Rh(PDOS). However, no magnetic instability of the Rh compound could be traced out in spin-polarized (SP) calculations.

Figure 4 shows the crystal orbital overlap populations (COOP) for the pair interactions accounting for the site multiplicities. As in Fig. 3, the energy is plotted relative to the Fermi level E_F. Major bonding occurs as expected from the above discussion within the T_2Si_2 layers. It is of a bonding nature (positive COOP magnitudes along the y axis), but starts to exhibit small antibonding contributions near E_F for the Rh compound. This follows from the Fermi level upshift in YRh_2Si_2. The Y–T bonding is also weak and not significantly different between the two compounds. However, a major difference going beyond the Fermi level upshift is shown by the large Y–Si bonding COOP in YRh_2Si_2. This follows the course of the Y–Si distances: 309 pm in YRh_2Si_2 *vs*. 320 pm in YRu_2Si_2.

Thus, while the electronic structures of YRu_2Si_2 and YRh_2Si_2 reveal similarities regarding their DOS shapes, the effect of the extra electron contributed by the Rh atoms is clearly evident.

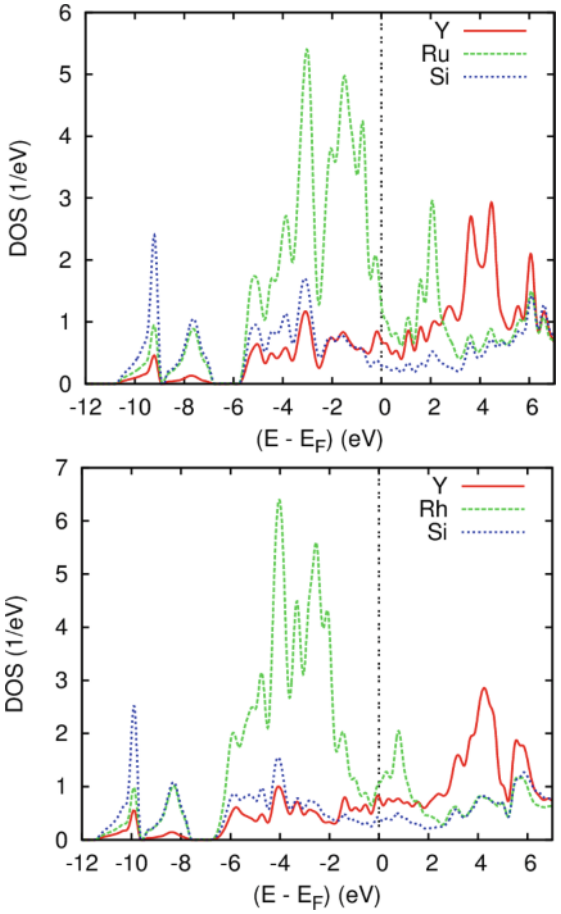

Fig. 3. (color online). Electronic density of states DOS. Site projected DOS (PDOS) of YRu_2Si_2 (top) and YRh_2Si_2 (bottom).

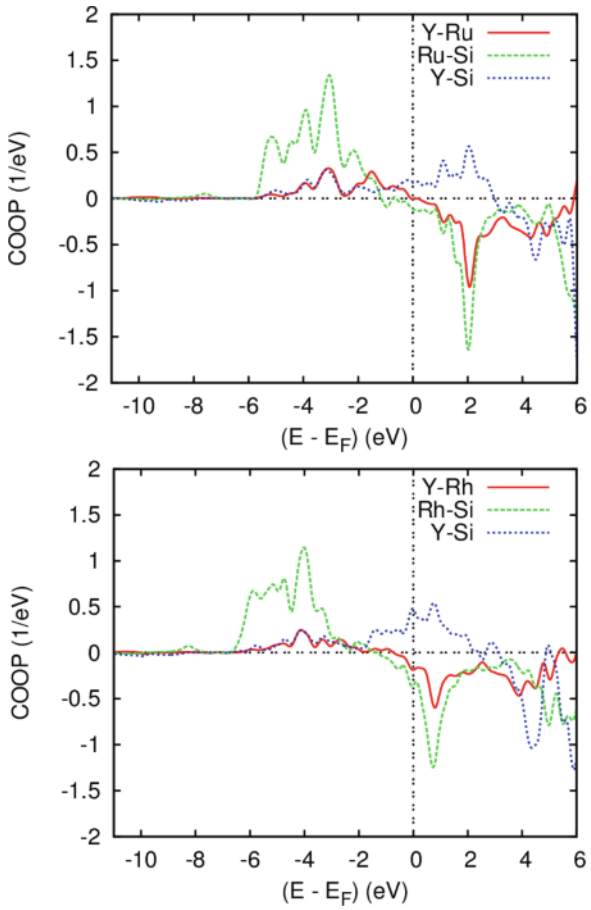

Fig. 4. (color online). Chemical bonding from overlap populations with the COOP criterion for the different interactions in YRu_2Si_2 (top) and YRh_2Si_2 (bottom).

^{89}Y solid-state NMR spectroscopy

Figure 5 and Table 5 summarize the solid-state NMR results. As expected, the spectra reveal single crystallographic yttrium sites, whose resonance shifts are highly dependent on the T atom present. Within both series of compounds involving T atoms of the 4th and 5th period, the Knight shift decreases systematically with increasing valence electron count. In addition, unsystematic variations in the line widths (full width at half maximum) are observed, which we attribute to variations in the extent of structural and electronic disorder caused by the synthetic procedure used. The particularly anomalous behavior shown by YRu_2Si_2 regarding its crystal chemistry is also seen in the ^{89}Y NMR data. This compound not only shows the highest Knight shift within the entire series, but also indicates a strong Knight shift anisotropy, as reflected by the strong spinning sideband intensities observed at integer multiples of the MAS rotation frequency. From an analysis of the peak intensity profile, the anisotropy parameters are estimated as $\delta = -650$ ppm and $\eta = 0.5$. None of the other compounds measured here gives any indication of a Knight shift anisotropy. A similar phenomenon was recently observed in a ^{89}Y NMR study of YTX compounds. While in YIrSn and in all $YNiX$ (X = Si, Ge, Sn) compounds the closest neighbors to yttrium are the transition metal atoms, an inverse situation is observed for YIrSi and YIrGe, where the Y–X distances are shorter than the Y–Ir distances. Significantly, only the latter two compounds reveal significant Knight shift anisotropies [44]. Thus, we may conclude that this particular NMR parameter is particularly sensitive to such site occupancy reversals.

Table 5. ^{89}Y MAS NMR fitting parameters of YT_2Si_2 (T = Co, Ni, Cu, Ru, Rh, Pd).

Compound	δ_{iso} (ppm)	Δ (Hz)
YCo_2Si_2	1521	825
YNi_2Si_2	832	2634
YCu_2Si_2	585	292
YRu_2Si_2	2131	682
YRh_2Si_2	1278	481
YPd_2Si_2	1013	537

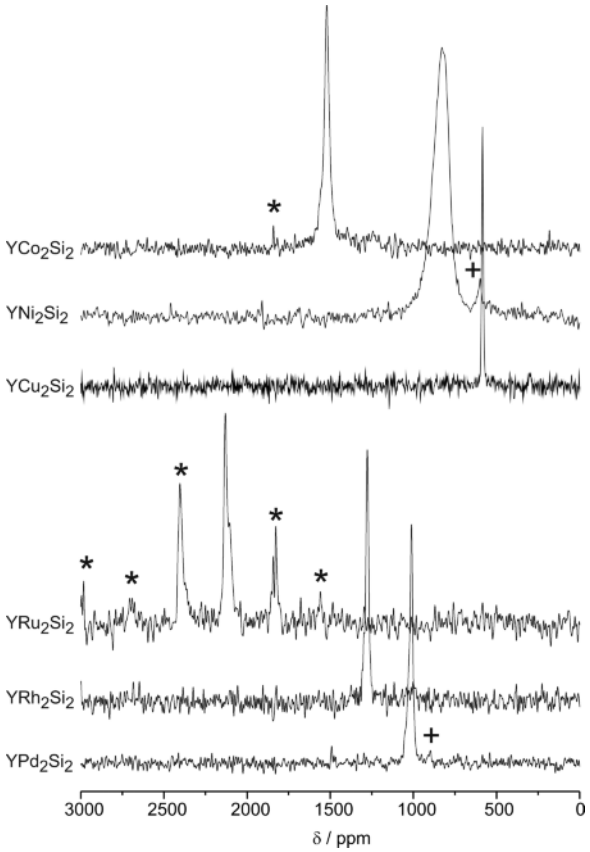

Fig. 5. 24.5 MHz ^{89}Y solid-state NMR spectra of the series of YT_2Si_2 (T = Co, Ni, Cu, Ru, Rh, Pd) silicides at room temperature (from top to bottom). Impurities and spinning sidebands are marked by crosses and asterisks, respectively.

Acknowledgement

This work was supported by the Deutsche Forschungsgemeinschaft.

[1] K. R. Andress, E. Alberti, *Z. Metallkd.* **1935**, *27*, 126.
[2] Z. Ban, M. Sikirica, *Acta Crystallogr.* **1965**, *18*, 594.
[3] P. Villars, K. Cenzual, *Pearson's Crystal Data – Crystal Structure Database for Inorganic Compounds*, (release 2013/14), ASM International, Materials Park, Ohio (USA) **2013**.
[4] A. Szytuła, J. Leciejewicz, *Handbook of Crystal Structures and Magnetic Properties of Rare Earth Intermetallics*, CRC Press, Boca Raton, **1994**.
[5] G. Just, P. Paufler, *J. Alloys Compd.* **1996**, *232*, 1.
[6] H. von Löhneysen, A. Rosch, M. Vojta, P. Wölfle, *Rev. Mod. Phys.* **2007**, *79*, 1015.

[7] P. Gegenwart, Q. Si, F. Steglich, *Nat. Phys.* **2008**, *4*, 186.
[8] R. Pöttgen, W. Hönle, H. G. von Schnering in *Encyclopedia of Inorganic Chemistry*, 2nd edition, (Ed.: R. B. King), Wiley, New York, **2005**, Vol. VII, pp. 4255.
[9] R. Hoffmann, C. Zheng, *J. Phys. Chem.* **1985**, *89*, 4175.
[10] C. Zheng, R. Hoffmann, *Z. Naturforsch.* **1986**, *41b*, 292.
[11] D. Johrendt, C. Felser, O. Jepsen, O. K. Andersen, A. Mewis, J. Rouxel, *J. Solid State Chem.* **1997**, *130*, 254.
[12] R. N. Shelton, H. F. Braun, E. Musick, *Solid State Commun.* **1984**, *52*, 797.
[13] M. Hirjak, P. Lejay, B. Chevalier, J. Etourneau, P. Hagenmuller, *J. Less-Common Met.* **1985**, *105*, 139.
[14] T. T. M. Palstra, G. Lu, A. A. Menovsky, G. J. Nieuwenhuys, P. H. Kes, J. A. Mydosh, *Phys. Rev. B* **1986**, *34*, 4566.
[15] M. Rotter, M. Tegel, D. Johrendt, *Phys. Rev. Lett.* **2008**, *101*, 107006.
[16] M. Rotter, M. Pangerl, M. Tegel, D. Johrendt, *Angew. Chem. Int. Ed.* **2008**, *120*, 8067.
[17] D. C. Johnston, *Adv. Phys.* **2010**, *59*, 803.
[18] C. Höting, H. Eckert, T. Langer, I. Schellenberg, R. Pöttgen, *J. Solid State Chem.* **2012**, *190*, 216.
[19] I. Felner, I. Nowik, *Solid State Commun.* **1983**, *47*, 831.
[20] K. Hiebl, P. Rogl, C. Horvath, K. Remschnig, H. Noël, *J. Appl. Phys.* **1990**, *67*, 943.
[21] C. S. Jee, B. Andraka, J. S. Kim, G. R. Stewart, *Phys. Rev. B* **1991**, *43*, 2656.
[22] K. Hiebl, C. Horvath, P. Rogl, M. J. Sienko, *J. Magn. Magn. Mater.* **1983**, *37*, 287.
[23] D. Rossi, R. Marazza, R. Ferro, *J. Less-Common Met.* **1978**, *58*, 203.
[24] W. Rieger, E. Parthé, *Monatsh. Chem.* **1969**, *100*, 444.
[25] H. Kido, T. Hoshikawa, M. Shimada, M. Koizumi, *Funtai oyobi Funmatsu Yakin* (*J. Jpn. Soc. Powder Powder Metall.*) **1984**, *31*, 67.
[26] B. Rupp, P. Rogl, F. Hulliger, *J. Less-Common Met.* **1987**, *135*, 113.
[27] N. D. Dung, H. Harima, Y. Onuki, T. D. Matsuda, S. Ikeda, E. Yamamoto, Y. Haga, Y. Takeda, T. Endo, Y. Doi, R. Settai, *J. Phys. Soc. Jpn.* **2008**, *77*, 094702.
[28] N. D. Dung, H. Harima, Y. Onuki, T. D. Matsuda, S. Ikeda, E. Yamamoto, Y. Haga, Y. Takeda, T. Endo, Y. Doi, R. Settai, *J. Phys. Soc. Jpn.* **2009**, *78*, 024712.
[29] O. I. Bodak, L. O. Muratova, I. R. Mokra, V. I. Yarovets, A. S. Sobolyev, E. I. Gladyshevskii, *Strukt. Faz* (*Fazovye Prevrashch. Diagrammy Sostoyaniya Met. Sist.*) **1974**, 182.
[30] R. V. Skolozdra, E. I. Gladyshevskii, *Inorg. Mater.* **1967**, *3*, 727.
[31] R. Ballestracci, *C. R. Séances Acad. Sci. (Ser. B)* **1976**, 282.
[32] R. Pöttgen, Th. Gulden, A. Simon, *GIT Labor-Fachzeitschrift* **1999**, *43*, 133.
[33] K. Yvon, W. Jeitschko, E. Parthé, *J. Appl. Crystallogr.* **1977**, *10*, 73.
[34] V. Petříček, M. Dušek, L. Palatinus, JANA2006, The Crystallographic Computing System, Institute of Physics, University of Prague, Prague (Czech Republic) **2006**.
[35] L. Palatinus, G. Chapuis, *J. Appl. Crystallogr.* **2007**, *40*, 786.
[36] P. Hohenberg, W. Kohn, *Phys. Rev.* **1964**, *136*, B864.
[37] W. Kohn, L. J. Sham, *Phys. Rev.* **1965**, *140*, A1133.
[38] J. Perdew, K. Burke, M. Ernzerhof, *Phys. Rev. Lett.* **1996**, *77*, 3865.
[39] A. R. Williams, J. Kübler, C. D. Gelatt, *Phys. Rev. B* **1979**, *19*, 6094.
[40] V. Eyert, *The Augmented Spherical Wave Method – A Comprehensive Treatment*, Lecture Notes in Physics, Springer, Heidelberg, **2007**.
[41] R. Hoffmann, *Angew. Chem., Int. Ed. Engl.* **1987**, *26*, 846.
[42] E. Parthé, L. Gelato, B. Chabot, M. Penzo, K. Cenzual, R. Gladyshevskii, TYPIX - *Standardized Data and Crystal Chemical Characterization of Inorganic Structure Types*, Gmelin Handbook of Inorganic and Organometallic Chemistry, 8th edition, Springer, Berlin **1993**.
[43] J. Emsley, *The Elements*, Oxford University Press, Oxford **1999**.
[44] C. Höting, H. Eckert, F. Haarmann, F. Winter, R. Pöttgen, to be published.